Supplementary information

High-temperature Stable hydroxyl Tuning the Local Environment of Pt Single Atom for Boosting Formaldehyde Oxidation

Mingyi Xiao[#a], Lina Zhang[#[b]], Shuzhe Zheng[#[a]], Ling Fang[a], Tulai Sun[a], Yonghe Li[a], Mingwu Tan[c], Jianghao Zhang[d], Yihan Zhu[a], Jinshu Tian[#*[a]], Haifeng Xiong*[b]

[a] College of Chemical Engineering, Zhejiang University of Technology, Hangzhou, 310014, China

[b] College of Chemistry and Chemical Engineering, State Key Laboratory for Physical Chemistry of Solid Surfaces, Xiamen University, Xiamen, 361005, China

[c] Institute of Sustainability for chemicals, Energy and Environment, Agency for Science, Technology and Research (A∗STAR), 1 Pesek Road, Jurong Island, 627833, Singapore

[d] State Key Joint Laboratory of Environment Simulation and Pollution Control, Research Center for Eco-environmental Sciences, Chinese Academy of Sciences, Beijing, 100085, China

* Corresponding authors: haifengxiong@xmu.edu.cn; tianjs@zjut.edu.cn

# These authors contributed equally to this work.

Characterizations

High-angle annular dark-field scanning transmission electron microscopy (HAADF-STEM)

High-angle annular dark-field scanning transmission electron microscopy (HAADF-STEM) images were recorded using a state-of-the-art transmission electron microscope (Thermo Scientific Spectra 300) equiped with double (image and probe) spherical aberration (Cs) correctors and operating at 300 kV.

X-ray Absorption Spectroscopy (XAS)

The XAS spectra at the Pt L3-edges were recorded at the BL11B beamline of Shanghai Synchrotron Radiation Facility (SSRF). The incident photons were monochromatized by a Si(111) double-crystal monochromator. The energy calibration was performed using a Pt reference foil. The reference spectra were measured in the transmission mode, while the *ex-situ* XAS spectra of the samples were measured in the fluorescence mode using a Lytle detector. The XAS spectra were analyzed using the Demeter software package [1]. The background subtraction and edge step normalization of the XAS raw data were performed using the Athena program. The k^3-weighted $\chi(k)$ data of the Pt L_3-edges spectra were Fourier transformed to real space using a hanning window. The Artemis program was used to obtain the quantitative structural parameters by least-squares fitting.

X-ray Photoelectron Spectroscopy (XPS)

The XPS measurements were carried out on Thermo Scientific K-Alpha with a focused monochromatic Al Kα X-ray (1486.6 eV) source and multi-channel detector.

The sample is prepared by taking an appropriate sample, pressing it into a paste, and mounting it onto the sample tray. The sample is then placed into the analysis chamber of a Thermo Scientific K-Alpha XPS instrument. The chamber pressure is reduced to less than 2.0×10^{-7} mbar before the sample analysis begins. The spot size of the analysis beam is 400 μm, and the working voltage is set to 12 kV with a filament current of 6 mA. The full spectrum scanning is performed with a step size of 1 eV and a scanning energy range of 150 eV. For the narrow-spectrum scanning, the step size is 0.1 eV and the scanning energy range is 50 eV.

Power X-ray diffraction (XRD)

X-ray diffraction (XRD) patterns were recorded with a PANalytical Empyrean powder diffractometer using Cu *Kα* radiation (λ= 0.1541 nm). The working voltage was 45 kV and the working current was 40 mA. The patterns were collected with a 2θ range from 10° to 80° at a step of 0.0167°.

Raman spectroscopy

Raman spectra were collected using an ID Spec ARCTIC confocal Raman system equipped with a holographic notch filter, a He-Ne laser (632.8 nm), and a CCD detector. The laser power is about 3 mW, and the spectral resolution is 2 cm^{-1}. For all Pt_1/CeO_2 catalysts, Raman tests were conducted at room temperature in static air. All the obtained spectra are displayed without smooth or baseline subtraction.

Diffuse Reflectance Infrared Fourier Transformed Spectroscopy (DRIFTS)

In situ Diffuse Reflectance Infrared Fourier Transformed Spectroscopy (DRIFTS) analysis was employed to investigate the adsorption behavior of CO molecules on Pt

species of the catalyst, as well as to monitor the dynamic change of the catalyst surface species on the catalysis during the HCHO reaction process. DRIFTS spectra were recorded using a ThermoFisher IS50 instrument quipped with a smart collector and a liquid N_2 cooled MCT detector, coupled with a Praying Mantis™ Diffuse Reflection accessory from Harrick. The spectra and backgrounds taken were averaged from 64 scans with a resolution of 4 cm^{-1}.

The test protocol for measuring the presence of surface hydroxyls on catalysts is as follows: the catalyst is pre-treated in a nitrogen (N_2) environment at a flow rate of 40 mL/min and at a temperature of 300°C for 60 minutes. Subsequently, the infrared spectrum is recorded at 50,100 and 300°C. Similarly, a KBr sample is processed under the same conditions and the resulting IR spectra are used as a background.

The procedure for DRIFTS during the CO adsorption (CO-DRIFTs) was reported in the previous work [2] and was briefly described as follows: the catalyst was pretreated at 350℃ for 30 min under 10% O_2/He with the flowrate of 40 $mL \cdot min^{-1}$, followed by purging with 40 $mL \cdot min^{-1}$ He for 15 min. After decreasing the temperature to 120℃, the background spectrum was taken at this temperature. Then, IR spectra were recorded. In the experiments, 1% CO /6% O_2 balanced with He was introduced into the cell (40 $mL \cdot min^{-1}$). After flowing the above CO/O_2/He mixture for 10 min, the CO was stopped, and the spectra were collected in the flowing 10% O_2/He for 10 min.

The procedure for DRIFTS during the HCHO oxidation reaction was also reported in our previous work [2]. Briefly, the sample was degassed using high purity N_2 (40 $mL \cdot min^{-1}$) at 200℃ for 1 h. After cooling to room temperature, the background

spectrum was collected. In the experiment, the gas containing 400 ppm HCHO/N_2 or 400 ppm HCHO/20% O_2/N_2 (total flow rate: 50 mL·min^{-1}) was used to performed the adsorption experiments.

CO temperature programmed reduction (CO-TPR)

The surface oxygen was determined by CO temperature programmed reduction (CO-TPR). CO-TPR was carried out on a homemade instrument, where 100 mg catalyst (40-60 mesh) was typically used in each test. First, the catalyst was oxidized in a N_2 (30 mL·min^{-1}) at 200℃ for 60 min, then cooled down to room temperature in the N_2 atmosphere. Next, 1% CO/He (30 mL·min^{-1}) was introduced. After the gas flow was stabilized, the temperature was ramped at 10 ℃·min^{-1} from room temperature to 600℃. The evolved CO_2 and H_2 were analyzed by a mass spectrometer (Pfeiffer Omni Star GSD 320).

Density functional theory calculations

The periodic density function theory (DFT) calculations were performed using the CP2K package [3, 4]. The exchange-correlation potential was described using the Perdew-Burke-Ernzerh (PBE) form of the generalized-gradient approximation (GGA) [5]. The wave functions were expanded in a molecularly optimized double-Gaussian basis set, with an auxiliary plane wave basis set with a cutoff energy of 400 Rydberg. The scalar relativistic norm-conserving pseudo-potentials were employed to modelled the core electrons [6] with 18, 12, 6, 4 and 1 valence electrons for Pt, Ce, O, C and H, respectively. The only Γ-point in reciprocal space mesh was used for integrating the Brillouin zone. The DFT+U method [7], based on the Mullikan 4f state population

analysis, was used to describe the Ce 4f electrons. A U value was set at ~4.1 eV in line with the previous literatures [8-10], which ensures that the redox property is reproduced correctly [11]. Grimme's third generation DFT-D3 approach was used to describe dispersion corrections [12]. The CeO_2 (111) was used to model the CeO_2 substrate, constructed with cell dimensions of 15.3442×13.2885×27.5285 Å with 15 Å vacuum space to minimize the interaction between slabs (Alpha, Beta and Gamma are all equal to 90^o). The convergence criterion used for geometry optimizations was a maximum force of 0.01 eV Å^{-1}. Spin polarization was considered in all calculations. The climbing image nudged elastic bands (CI-NEB) method with seven intermediate images along the reaction pathway between initial and final states was used to locate transition states of elementary steps. steps [13, 14]. To get the different vibrational modes of CO molecule, the vibrational analysis for different models was carried out in the harmonic approximation using finite difference with displacements of magnitude 0.01 Å.

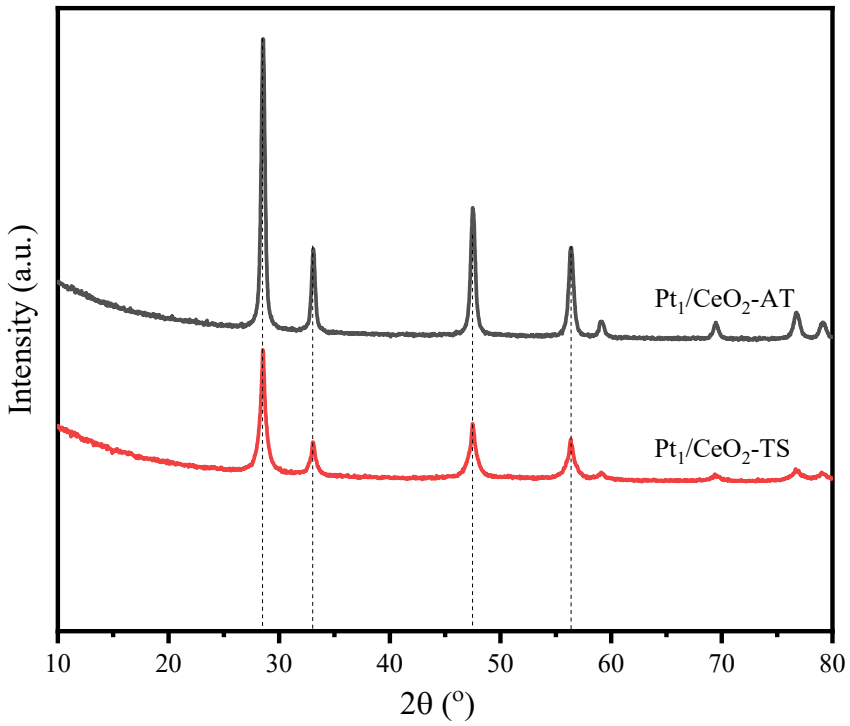

Fig. S1. Powder X-ray diffraction (XRD) patterns of Pt_1/CeO_2-AT and Pt_1/CeO_2-TS catalysts.

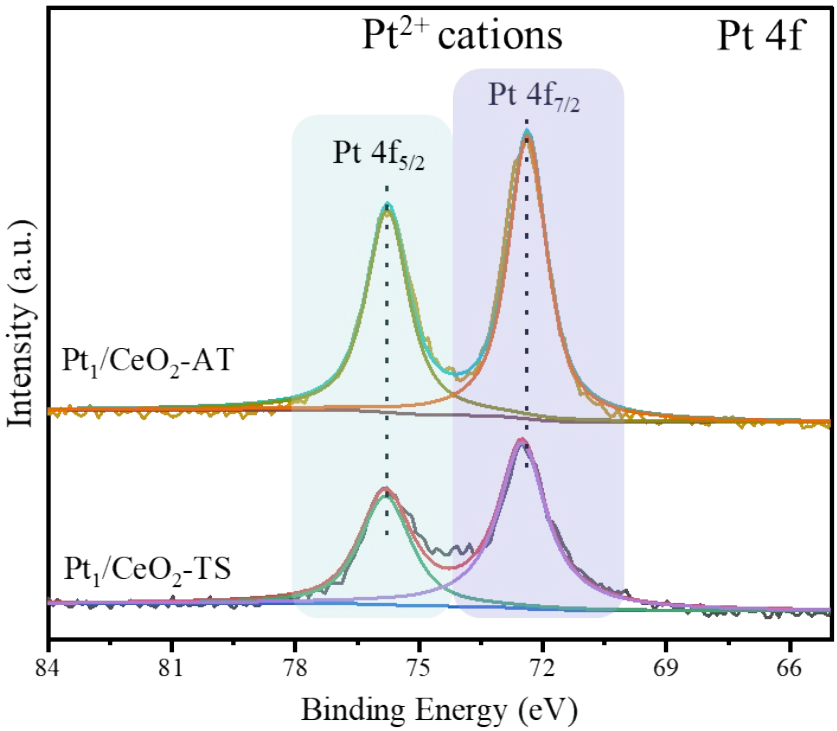

Fig. S2. X-ray photoelectron spectroscopy results of Pt_1/CeO_2-AT and Pt_1/CeO_2-TS catalysts in the Pt 4f region

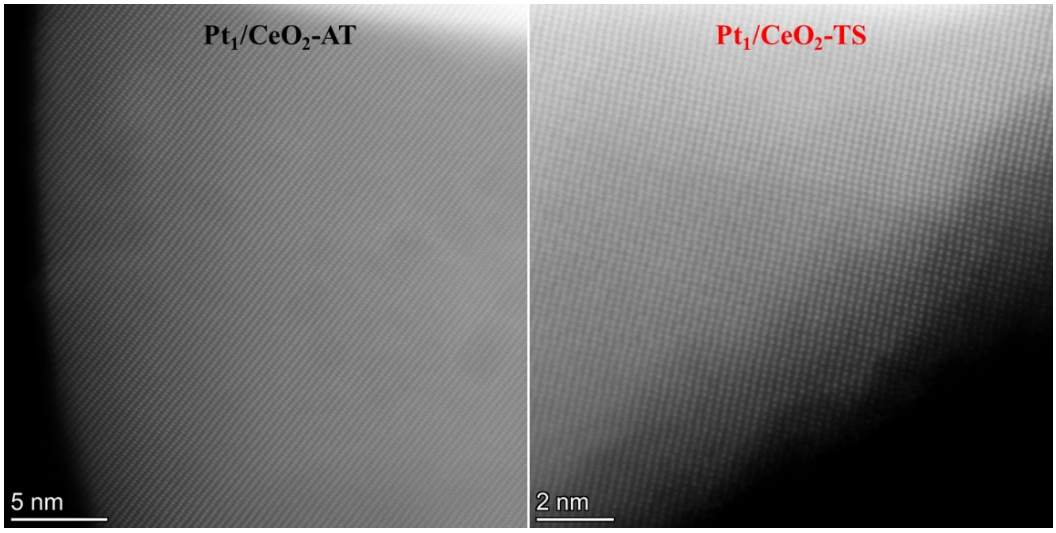

Fig. S3. HAADF-STEM images of Pt_1/CeO_2-AT and Pt_1/CeO_2-TS showing the exclusive presence of isolated Pt atoms

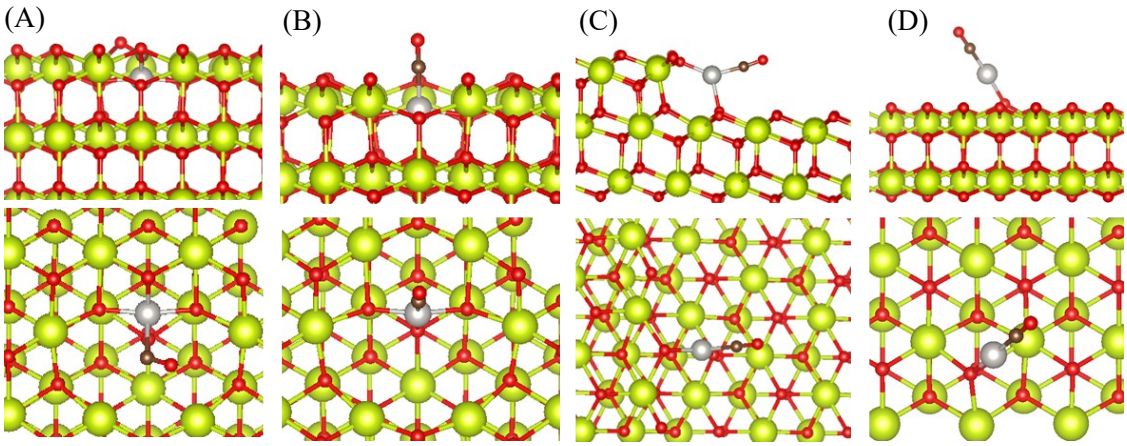

Fig. S4. The different structural models correspond to the different vibrational frequencies. (A) Pt_1/CeO_2 (111) sample (CN=4) with CO vibrational frequency at 2123.7 cm^{-1}; (B) Pt_1/CeO_2 (111) sample (CN=3) with CO vibrational frequency at 2078.4 cm^{-1}; (C) Pt_1/CeO_2 (111) sample (CN=2) with CO vibrational frequency at 2058.6 cm^{-1}; (D) Pt_1/CeO_2 (111) sample (CN=1) with CO vibrational frequency at 2028.2 cm^{-1}.

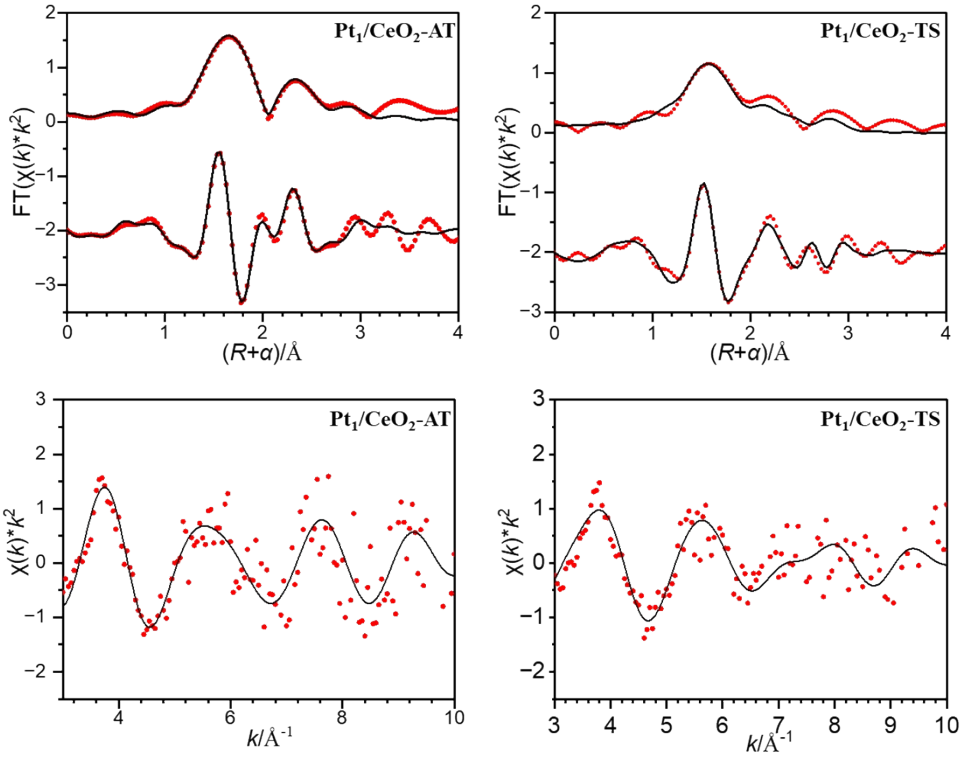

Fig. S5. Best fitting of the Pt-L_3 EXAFS results in R space and K space of the Pt_1/CeO_2-AT and Pt_1/CeO_2-TS catalysts.

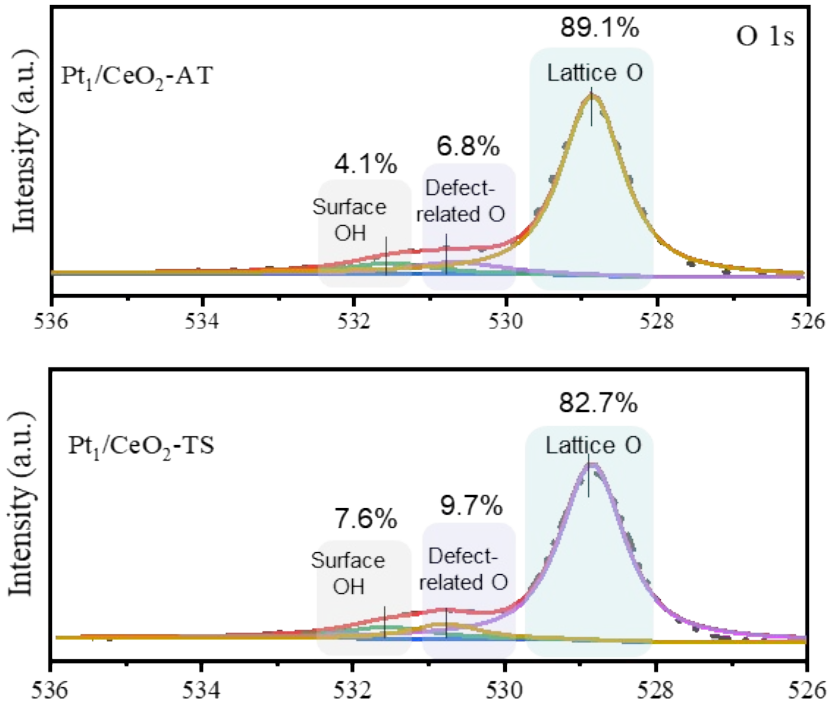

Fig. S6. X-ray photoelectron spectroscopy results of Pt_1/CeO_2-AT and Pt_1/CeO_2-TS catalysts in the O 1s region.

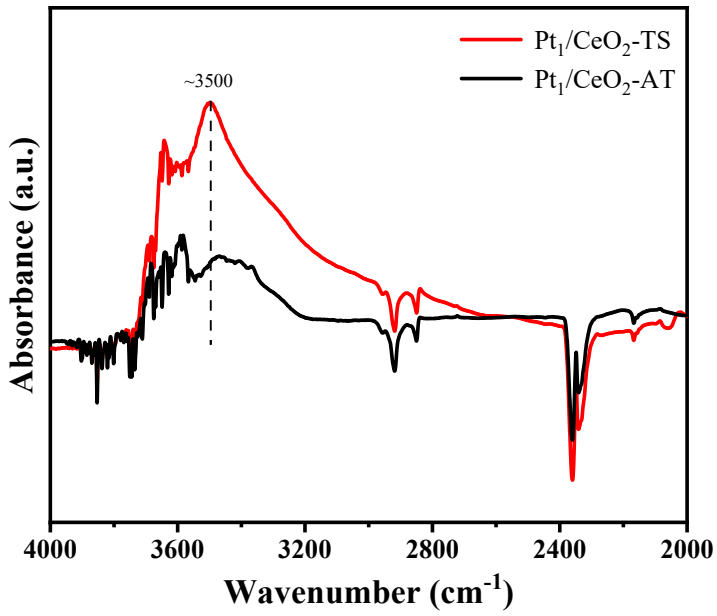

Fig. S7. *In-suit* FTIR spectra of Pt_1/CeO_2-AT and Pt_1/CeO_2-TS catalysts at 300°C.

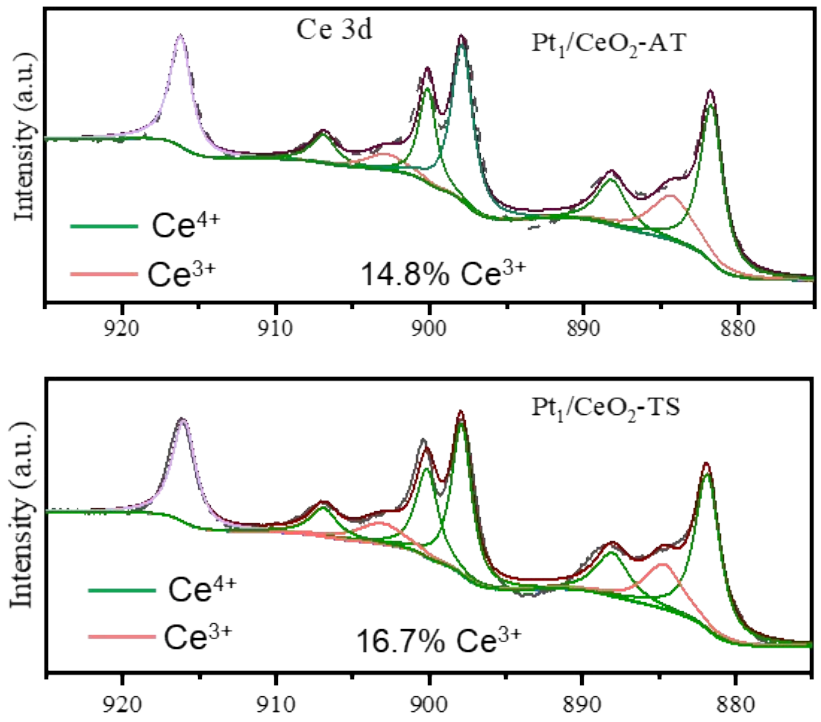

Fig. S8. X-ray photoelectron spectroscopy results of Pt_1/CeO_2-AT and Pt_1/CeO_2-TS catalysts in the Ce 3d region.

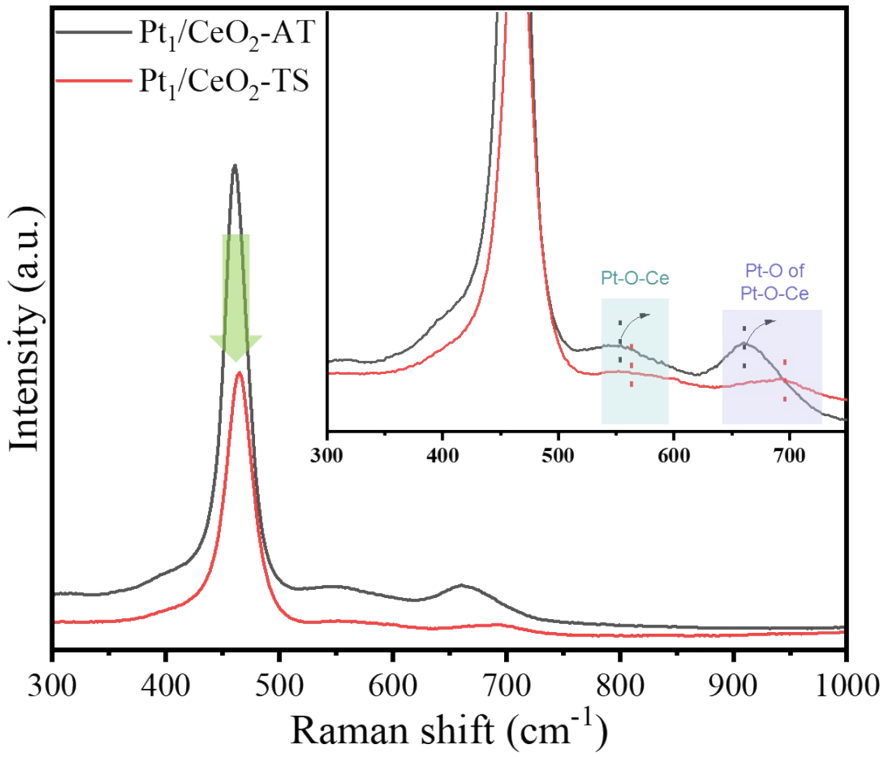

Fig. S9. Raman spectra of Pt_1/CeO_2-AT and Pt_1/CeO_2-TS catalysts

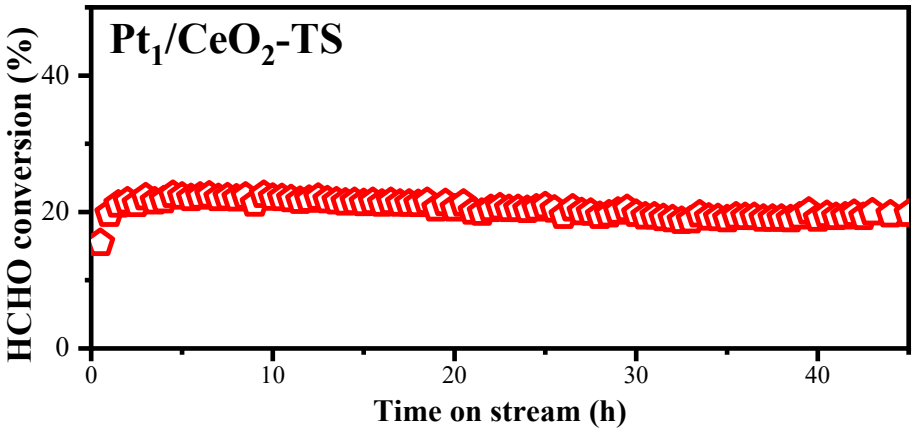

Fig. S10. HCHO conversion as a function of time on stream on Pt_1/CeO_2-TS catalyst at 30℃. **Reaction condition**: 400 ppm HCHO, 20 vol% O_2, and N_2 as balance gas, total flow rate: 50 mL·min^{-1}, WHSV: 60,000 mL·g^{-1}·h^{-1}.

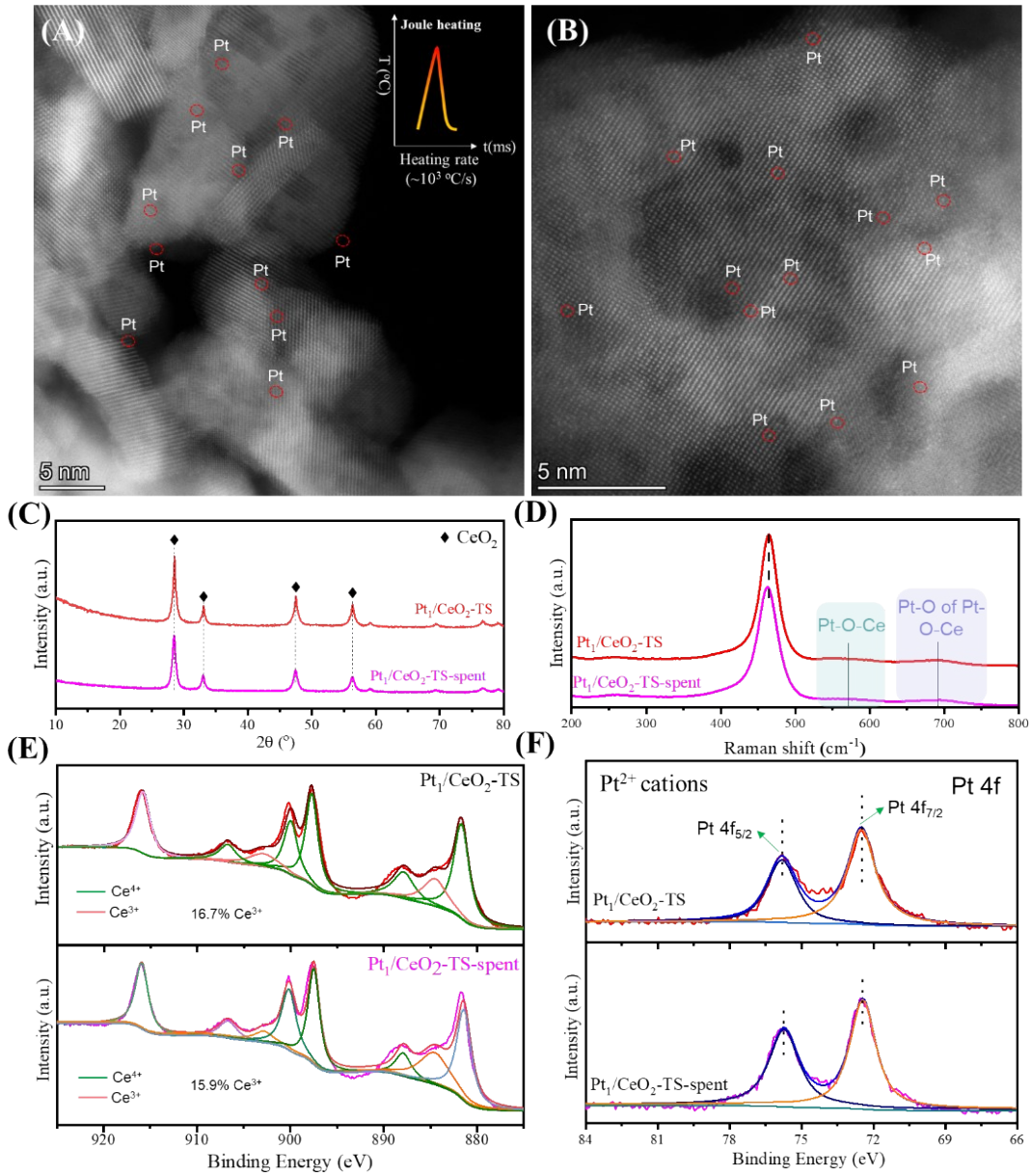

Fig. S11. Structural characterization of catalyst before and after reaction**.** (A-B) STEM images of Pt_1/CeO_2-TS catalyst before and after HCHO oxidation; (C) Powder X-ray diffraction (XRD) patterns of Pt_1/CeO_2-TS catalysts before and after HCHO oxidation; (D) Raman spectra of Pt_1/CeO_2-TS catalysts before and after HCHO oxidation; (E-F) X-ray photoelectron spectroscopy results of Pt_1/CeO_2-TS catalysts in the Ce 3d (E) and Pt4f (F) regions before and after HCHO oxidation. Reaction condition: 400 ppm HCHO, 20 vol% O_2, and N_2 as balance gas, total flow rate: 100 mL·min^{-1}, WHSV: 60,000 mL·g^{-1}·h^{-1}

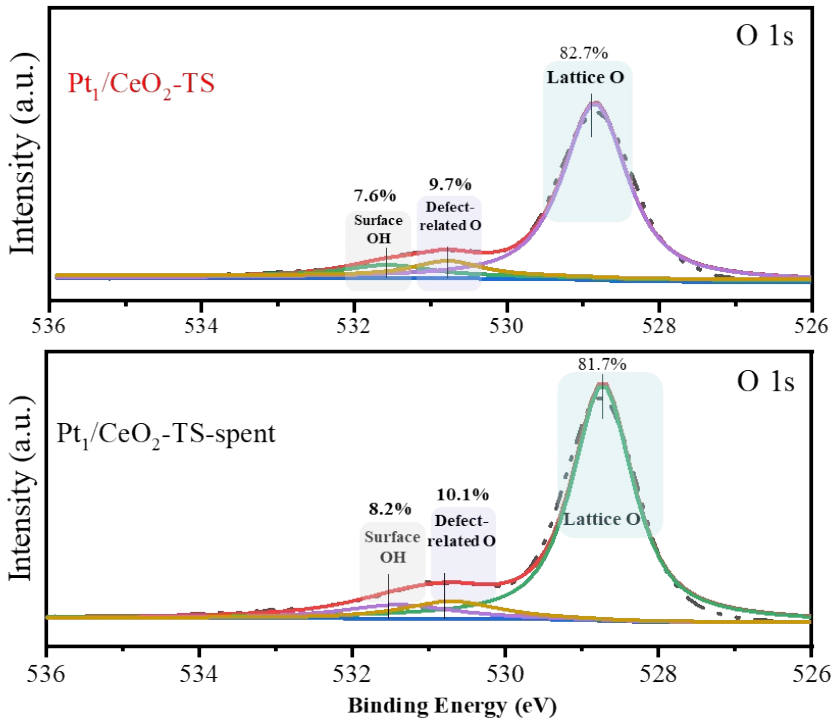

Fig. S12. X-ray photoelectron spectroscopy results of Pt_1/CeO_2-TS catalysts in the O1s regions before and after HCHO oxidation

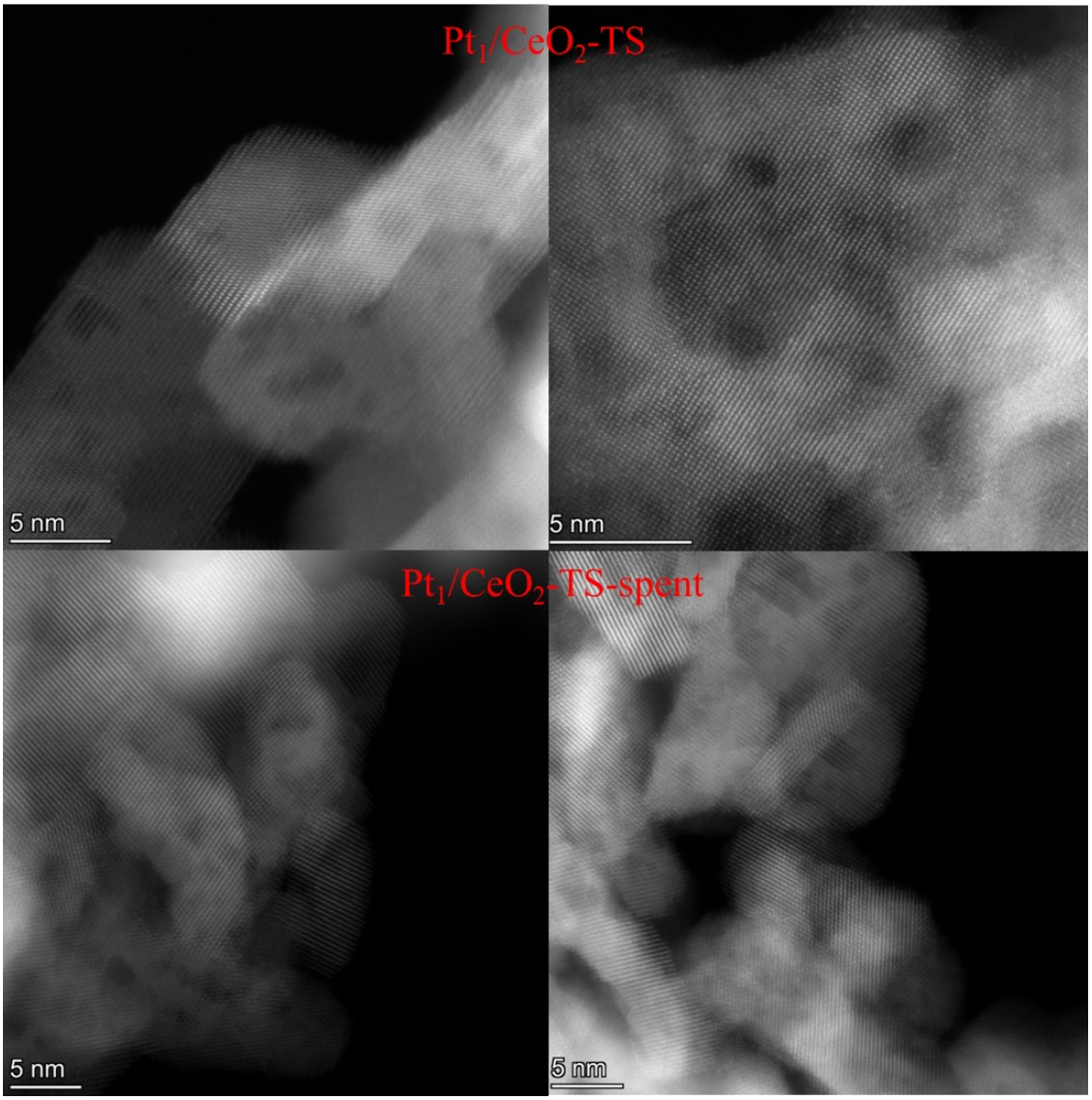

Fig. S13. STEM images of Pt_1/CeO_2-TS catalyst before and after HCHO oxidation in different regions.

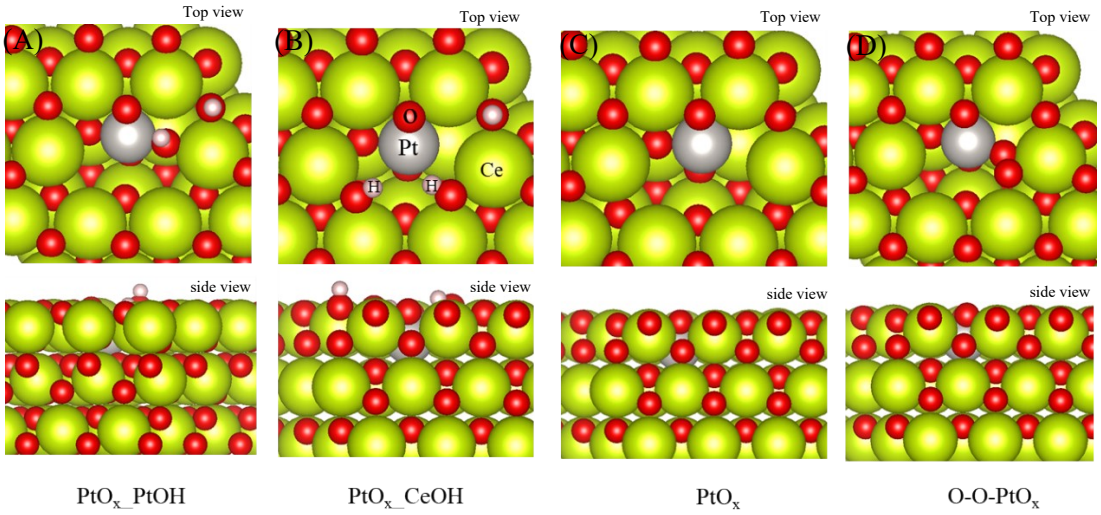

Fig. S14. The potential structural models to simulation the active site of Pt_1/CeO_2-TS catalyst. (A) PtO_4H; (B): PtO_3-OH; (C) PtO_3; (D): PtO_3-O_2. Although A structure has hydroxyl groups, its coordination number is roughly 4, which does not match the results obtained from the EXAFS analysis. The D structure, which may exist under oxidizing conditions, is unlikely to be the initial structure of the reaction. The B structure is able to satisfy the coordination number and is consistent with the presence of hydroxyl groups. The C structure is used as a control to investigate the role of hydroxyl groups in the reaction process.

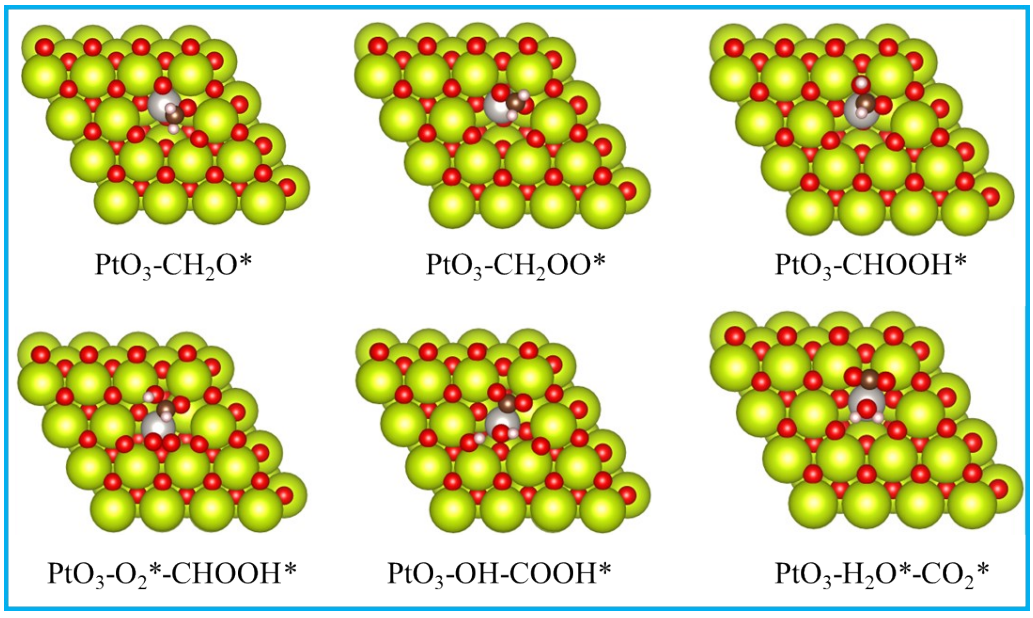

Fig. S15 Optimizing the Geometric Structure of the Formaldehyde Oxidation Process on a PtO_3 Model.

Table S1. Grain and particle sizes estimated from XRD and BET surface areas of Pt_1/CeO_2-AT, Pt_1/CeO_2-TS and Pt_1/CeO_2-TS-spent.

Samples	Grain size (nm)	Special surface area (m^2/g)	Pt loading (wt%)[a]
Pt_1/CeO_2-AT	22	32	0.95
Pt_1/CeO_2-TS	12	61	0.97
Pt_1/CeO_2-TS-spent	11	59	0.95

[a] Collected from ICP-AES (Thermo iCAP 6300, Thermo Fisher Scientific).

The surface area of Pt_1/CeO_2-TS (61 m^2/g) is higher than that of Pt_1/CeO_2-AT (32 m^2/g), which is consistent with the earlier reports that the ultrafast pulse heating and cooling helps preserve the surface area of the CeO_2 support (Angewandte Chemie, 60 (2021) 26054-26062).

Table S2. Best fitting results of EXAFS over Pt_1/CeO_2-AT and Pt_1/CeO_2-TS.

Samples	Scattering pair	CN[a]	R/Å[b]	σ^2/Å^{2c}	R factor
Pt_1/CeO_2-AT	Pt-O	4.2	2.013	0.0012	0.023
Pt_1/CeO_2-TS	Pt-O	3.6	1.962	0.0042	0.047

[a]CN is the coordination number.

[b]R is interatomic distance (the bond length between Pd central atoms and surrounding coordination atoms).

[c]σ^2 is Debye-Waller factor (a measure of thermal and static disorder in absorber scatterer distances).

Table S3. Summary of catalytic properties of some representative Pt-based formaldehyde oxidation catalysts

Catalysts	Space velocity (mL/h.g)	Gas composition	R.T. HCHO conversion (%)	Turnover frequencies (h^{-1})	Ref.
Pt-$0.3FeO_x/Al_2O_3$	60000	~300 ppm HCHO, ~30%RH	63	4.92	RSC Advances,**5 (**2015), 104330-104336
Pt/MnO_2	20000	~ 460 ppm HCHO	30	1.20	The Journal of Physical Chemistry C 116.1 (2012): 851-860.
Pt/MnO_x-CeO_2	30000	~30 ppm HCHO	100	2.63	Applied Catalysis B: Environmental, 81(2008): 115-121.
Pt/TiO_2	30000	~50 ppm HCHO, ~35%RH	100	3.26	Chinese Journal of Catalysis 38.2 (2017): 199-206
$PtNi/Al_2O_3$	48000	~30 ppm HCHO, ~35%RH	90	5.65	Applied Catalysis B: Environmental 200 (2017): 543-551.
Pt/TiO_2	120,000	24 ppm HCHO, RH 54%	96	1.44	Applied Catalysis B: Environmental, 163 (2015), 436-443.
Pt_1/CeO_2-TS	37500	~460 ppm HCHO, RH,50%	65	8.49	This work

RT: Room temperature; RH: relative humidity

Table S4. IR bands after the adsorption of HCHO on the Pt_1/CeO_2-TS catalyst.

Species	Vibrational modes	IR bands wavenumber/cm^{-1}
DOM[a]	ν(OCO)	1065, 1085, 1124
	ν(CO)	945
HCOO[b]	ν_{as}(OCO)	1575
	δ(CH)	1370
	ν_s(OCO)	1355
C-H (HCOO/DOM)	ν_s(OCO)+δ(CH)	2749, 2803,2815, 2837, 2868, 2896,
	ν(CH)	2915
OH	ν(OH)	3695

[a] DOM = dioxymethylene

[b] HCOO = formate species

References

[1] B. Ravel, M. Newville, ATHENA, ARTEMIS, HEPHAESTUS: data analysis for X-ray absorption spectroscopy using IFEFFIT, Journal of synchrotron radiation, 12 (2005) 537-541.
[2] L. Zhang, B. Zhang, P. Xue, J. Li, Z. Zhang, Y. Yang, S. Wang, J. Lin, H. Liao, Y. Wang, Y. Yao, S. Wan, H. Xiong, The Effect of Pretreatment on the Reactivity of Pd/Al_2O_3 in Room Temperature Formaldehyde Oxidation, ChemCatChem, 13, (2021), 4133-4141..
[3] G. Lippert, J. Hutter, M. Parrinello, The Gaussian and augmented-plane-wave density functional method for ab initio molecular dynamics simulations, Theoretical Chemistry Accounts, 103 (1999) 124-140.
[4] J. VandeVondele, M. Krack, F. Mohamed, M. Parrinello, T. Chassaing, J. Hutter, Quickstep: Fast and accurate density functional calculations using a mixed Gaussian and plane waves approach, Computer Physics Communications, 167 (2005) 103-128.
[5] J.P. Perdew, K. Burke, M. Ernzerhof, Generalized gradient approximation made simple, Physical Review Letters, 77 (1996) 3865.
[6] S. Goedecker, M. Teter, J. Hutter, Separable dual-space Gaussian pseudopotentials, Physical Review B, 54 (1996) 1703.
[7] S.L. Dudarev, G.A. Botton, S.Y. Savrasov, C. Humphreys, A.P. Sutton, Electron-energy-loss spectra and the structural stability of nickel oxide: An LSDA+U study, Physical Review B, 57 (1998) 1505.
[8] Y.-G. Wang, D. Mei, V.-A. Glezakou, J. Li, R. Rousseau, Dynamic formation of single-atom catalytic active sites on ceria-supported gold nanoparticles, Nature communications, 6 (2015) 6511.
[9] Y.-G. Wang, D. Mei, J. Li, R. Rousseau, DFT+ U study on the localized electronic states and their potential role during H2O dissociation and CO oxidation processes on CeO_2 (111) surface, The Journal of Physical Chemistry C, 117 (2013) 23082-23089.
[10] H.T. Chen, J.G. Chang, H.L. Chen, S.P. Ju, Identifying the O_2 diffusion and reduction mechanisms on CeO_2 electrolyte in solid oxide fuel cells: a DFT+ U study, Journal of computational chemistry, 30 (2009) 2433-2442.
[11] Y.-G. Wang, Y. Yoon, V.-A. Glezakou, J. Li, R. Rousseau, The role of reducible oxide–metal cluster charge transfer in catalytic processes: new insights on the catalytic mechanism of CO oxidation on Au/TiO_2 from ab initio molecular dynamics, Journal of the American Chemical Society, 135 (2013) 10673-10683.
[12] S. Grimme, J. Antony, S. Ehrlich, H. Krieg, A consistent and accurate ab initio parametrization of density functional dispersion correction (DFT-D) for the 94 elements H-Pu, The Journal of Chemical Physics, 132 (2010) 154104.
[13] G. Henkelman, B.P. Uberuaga, H. Jonsson, A climbing image nudged elastic band method for finding saddle points and minimum energy paths, Journal of Chemical Physics, 113 (2000) 9901-9904.
[14] G. Mills, H. Jonsson, G.K. Schenter, REVERSIBLE WORK TRANSITION-STATE THEORY - APPLICATION TO DISSOCIATIVE ADSORPTION OF HYDROGEN, Surface Science, 324 (1995) 305-337.